Title

Ultrastable actinide endohedral borospherenes

Journal

Chemical Communications, 54(18)

ISSN

1359-7345

Authors

Wang, Cong-Zhi

Bo, Tao

Lan, Jian-Hui

et al.

Publication Date

2018-02-27

DOI

10.1039/c7cc09837e

Ultrastable Actinide Endohedral Borospherenes: U@B_{36} and Th@B_{38}

Cong-Zhi Wang,[a] Tao Bo,[a] Jian-Hui Lan,[a] Qun-Yan Wu,[a] Zhi-Fang Chai,[a,b] John K. Gibson,[c] and Wei-Qun Shi*[a]

Abstract: Since the discovery of the first all-boron fullerenes $B_{40}^{-/0}$, metal-doped borospherenes have been received extensive attention. So far, in spite of theoretical efforts on metalloborospherenes, the feasibility of actinide analogues remains minimally explored. Here we report a series of actinide borospherenes AnB_n (An=U, Th; *n*=36, 38, 40) from extensive first-principles theory calculations. All the AnB_n complexes are found to possess endohedral structures ($An@B_n$) as the global minima. In particular, U@B_{36} (C_{2h}, ^3A_g) and Th@B_{38} (C_{2h}, ^3B_u) exhibit nearly ideal endohedral borospherene structures. The C_{2h} U@B_{36} and Th@B_{38} complexes are predicted to be highly robust both thermodynamically and dynamically. In addition to the actinide size match to the cage, the covalent character of the metal-cage bonding in U@B_{36} and Th@B_{38} affords further stabilization. Bonding analysis indicates that the C_{2h} Th@B_{38} exhibits 3D aromaticity with σ plus π double delocalization bonding. The results demonstrate that doping with appropriate actinide atoms is promising to stabilize diverse borospherenes, and may provide routes for borospherene modification and functionalization.

Since the recent observation of the first all-boron fullerenes (D_{2d} $B_{40}^{-/0}$) in 2014,[1] the chemistry of borospherenes has developed rapidly.[2-5] Other subsequently reported borospherenes include B_{39}^-,[2] B_{38}^{2-},[3] B_{36}^{4-},[4] and B_{38}[6]. Metal doping has been used to modify the chemical bonding and to functionalize fullerenes,[7] and the slightly smaller diameter of borospherenes (e.g. B_{40}) relative to C_{60} render them candidates to dope with metal atoms. Recently, Li and co-workers[8] explored the first metalloborospherenes, MB_{40} (M = Be, Mg, Ca, Sr), at the density functional theory (DFT) level. Ca@B_{40} and Sr@B_{40} are predicted to exhibit almost perfect endohedral borospherene geometries, while M&B_{40} (M = Be, Mg) prefer exohedral borospherene structures. Subsequently, computational reports of other metalloborospherenes have appeared, including Ca@B_{38}[3] and Ca@B_{39}^+[9] with a Ca^{2+} ion at the centers of B_{38}^{2-} and B_{39}^- cages. Based on first-principles theory calculations, the Saturn-like complexes Li_4&B_{36}, Li_5&B_{36}^+, and Li_6&B_{36}^{2+} comprising a perfect cage-like B_{36}^{4-} were identified as viable.[4] In addition to alkaline earth and alkali metal atoms, it is predicted that borospherene cages are stabilized by doping the insides of the cages with transition metal and lanthanide metal atoms.[10-12] Jin et al.[10] presented a computational investigation of endohedral borospherenes M@B_{40} (M = Sc, Y, La). Lu et al.[11] reported a computational study of endohedral M@B_{38} (M = Sc, Y, Ti) and exohedral M&B_{38} (M = Nb, Fe, Co, Ni) fullerenes with a neutral B_{38} cage. It has been predicted that the d-block transition metal atoms (M = Ti, Zr, Hf, Cr, Mo, W, Fe, Ru and Os) demonstrate the ability to stabilize the small cage-like boron cluster B_{24}.[12] The possibility of the metalloborospherenes arouses our interest in more diverse metal-doped borospherenes. Despite the substantial attention to metalloborospherenes, there is so far no evidence for stabilization of boron cages by actinide metal atoms, except for the recently reported boron cluster U@B_{40}[13], rendering as fascinating the question of whether other actinide metal-doped borospherenes are viable. Here we assess the feasibility of synthesizing actinide metalloborospherenes AnB_n (An=U, Th; *n*=36, 38, 40) using extensive first-principles theory calculations. The results demonstrate that the encapsulated uranium and thorium atoms can stabilize boron cages, and the global minima of U@B_{36} (C_{2h}, ^3A_g) and Th@B_{38} (C_{2h}, ^3B_u) exhibit nearly ideal endohedral borospherene structures. Analogous to Ca@B_{40}[8], Th@B_{38} has σ plus π double delocalization. This work enriches and expands metalloborospherene chemistry to the realm of actinoborospherenes, and affords key insights for chemical modification and functionalization of borospherenes.

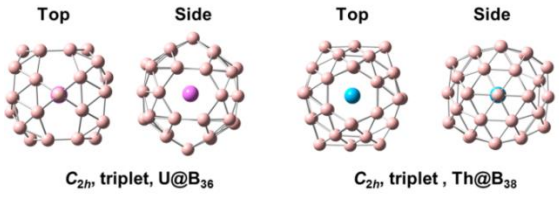

[a] Dr. C.-Z. Wang, Dr. T. Bo, Dr. J.-H. Lan, Dr. Q.-Y. Wu, Prof. Z.-F. Chai, Prof. W.-Qun Shi
Laboratory of Nuclear Energy Chemistry and Key Laboratory for Biomedical Effects of Nanomaterials and Nanosafety
Institute of High Energy Physics, Chinese Academy of Sciences, Beijing 100049, China
E-mail: shiwq@ihep.ac.cn
[b] Prof. Z.-F. Chai
School for Radiological and interdisciplinary Sciences (RAD-X) and Collaborative Innovation Center of Radiation Medicine of Jiangsu Higher Education Institutions
Soochow University, Suzhou 215123, China
[c] Dr. J. K. Gibson
Chemical Sciences Division
Lawrence Berkeley National Laboratory, Berkeley, California 94720, United States

Supporting information for this article is given via a link at the end of the document.

Figure 1. Optimized structures of C_{2h} U@B_{36} and C_{2h} Th@B_{38} at the PBE0/RECP/6-311+G* level of theory. Light pink, pink, and blue spheres represent B, U and Th, respectively.

Over 500 isomers of each actinide metal-doped borospherenes were found by global structural searches. The predicted ten low-lying isomers along with the low-lying exohedral structures of six studied AnB_n at the hybrid DFT–PBE0 level are displayed in Figures S1-S6, Supporting Information. Notably, all the global minimum isomers have endohedral metalloborospherene structures (An@B_n), while the exohedral structures (An&B_n) are much higher in energy. For each species, the lowest energy structures are well-defined with alternative structures being ~0.4 eV higher in energy at the PBE0 level. The global minimum structures of U@B_{36} and Th@B_{38} are particularly intriguing, having triplet configurations adopting relatively high symmetry (C_{2h}) with U and Th residing exactly at the boron cage centers (Figure 1). In contrast, Th@B_{36} exhibits a singlet structure with low C_i symmetry. The global minimum of B_{36} has a quasi-planar hexagonal geometry with the C_{2h} B_{36} cage lying 2.84 eV (PBE0) higher in energy. It is thus concluded that doping with endohedral U or Th stabilizes the cage-like isomer of B_{36}. In U@B_{38}, U@B_{40}, and Th@B_{40}, the U and Th atoms are far from the centers of the B_{38} and B_{40} cages, which are distorted relative to the corresponding hollow borospherenes reported previously.[1, 6] The calculated relative energies for the low-lying isomers are within 0.4 eV at the TPSSh and PDE0 levels (Figures S1-S6). Most significantly, the PBE0 and TPSSh results predict the same ground-state structure in each case. Spin-orbit (SO) coupling effects on the energy levels of these species were assessed for the representative complex C_{2h} U@B_{36} (Figure S7). Our calculations show that the MO splittings are overall small and the ground-state properties change only slightly due to SO effects.

In view of the fact that the U and Th atoms doped into different B_n cages exhibit various configurations of AnB_n, it is possible to assess the atomic size effect. For the metalloborospherenes of B_{40}, Li and co-workers[8] have confirmed that Sr doping favors the endohedral configuration with perfect D_{2d} symmetry. In comparison with Sr (2.15 Å), the atomic radii[14] of actinides U (1.56 Å) and Th (1.79 Å) are much smaller for the B_{40} cage and should thus not fill the B_{40} cage to the same degree as Sr. It is thus reasonable that U@B_{40}, and Th@B_{40} have irregular geometries based on our calculations. Similarly, U is evidently too small to reside in the center of an undistorted B_{38} cage, while Th is too large for the B_{36} cage that well accommodates U. Endohedral U and Th atoms are almost ideal size matches for the B_{36} and B_{38} cages, respectively. In the following discussions, we focus on the nearly geometrically ideal C_{2h} actinide borospherenes, U@B_{36} and Th@B_{38}.

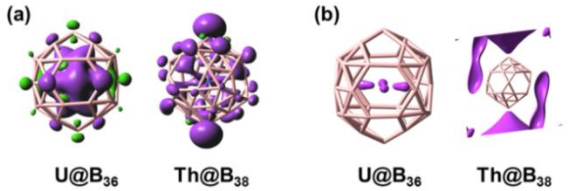

Figure 2. Isosurface plots of (a) spin density (0.002) and (b) spin polarization parameter (0.2, 0.4) function of U@B_{36} and Th@B_{38}.

For C_{2h} U@B_{36} and Th@B_{38}, the U-B and Th-B bond distances are in the ranges of 2.72~3.07 and 2.78~3.31 Å, respectively, which appear to be greater than the sum of the single-bond covalent radii of U (1.70 Å), or Th (1.75 Å) and B (0.85 Å).[15] This is reasonable given that the many An-B bonds cannot be full single bond character. The U@B_{36} and Th@B_{38} have fairly high SOMO–LUMO energy gaps of 2.8 and 1.6 eV, respectively. Electron density based population schemes, such as Voronoi deformation density (VDD)[16] and Hirshfeld[17] charge analyses, are employed to evaluate f-element atomic charges.[18-19] For U@B_{36} and Th@B_{38}, the VDD and Hirshfeld charges, respectively, on U are 0.604 e and 0.656 e, and on Th are 0.333 e, 0.418 e. This indicates that the actinides serve as electron donors to the boron cages, in line with the higher electronegativity of B versus U and Th. Mulliken population analysis shows that the atomic spin populations of U and Th are 1.967 and 0.125, respectively, indicating that the unpaired electrons mainly reside on the uranium atom in U@B_{36}, whereas they are predominantly on boron atoms in Th@B_{38}, especially on the two B atoms far away from the central thorium atom (Th-B distances: ~3.3 Å) with spin populations of about 0.5. These trends can be clearly observed by the isosurface plots of the spin density and spin polarization parameters (the ratio of unpaired electron density relative to total electron density) of U@B_{36} and Th@B_{38} (Figure 2).

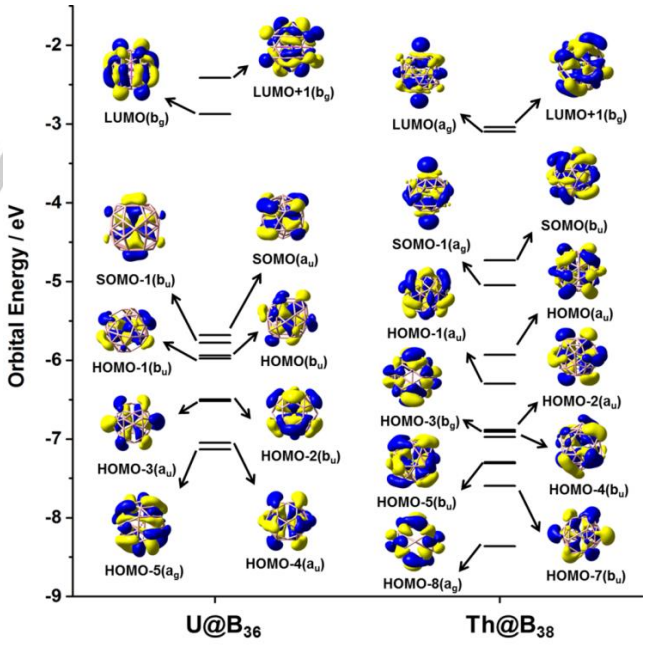

Figure 3. The frontier molecular orbitals of C_{2h} U@B_{36} and C_{2h} Th@B_{38}

To afford further insight into the thermodynamic stability of C_{2h} U@B_{36} and Th@B_{38}, we calculated the association energies relative to separated U + B_{36} (C_{6v}) and Th + B_{38} (D_{2h}) at the PBE0

level. The association energies of U@B_{36} and Th@B_{38} are predicted to be -210 and -221 kcal/mol, respectively, which are much more negative than reported for endohedral M@B_{40} (M = Ca, Sr)[8] and M@B_{38} (M = Sc, Y, Ti)[11]. These extremely high energies indicate the exceptional stabilities of U@B_{36} and Th@B_{38}, and substantial interactions between the actinides and the borospherenes. Molecular dynamics (MD) simulations were carried out to evaluate the dynamic stabilities of C_{2h} U@B_{36} and Th@B_{38}. As shown in Figures S8 and S9, U@B_{36} and Th@B_{38} are dynamically stable at 300 and 500 K for the 30 ps duration, with the root-mean-square-deviations (RMSD) of 0.10, 0.12 and 0.10, 0.25 Å (on average), respectively. These results show that U@B_{36} and Th@B_{38} are highly robust at least up to 500 K.

The exceptional stability of U@B_{36} and Th@B_{38} further spurs interest in nature of the metal-boron cage, particularly given the relatively long U-B and Th-B distances. To elucidate the electronic properties of the metal-boron bonding, MO analyses of C_{2h} U@B_{36} and C_{2h} Th@B_{38} were carried out at the PBE0/RECP/6-311+G* level of theory, and the Kohn–Sham frontier MOs are displayed in Figure 3. The MO plots give a pictorial description of the metal-ligand bonding, which suggests covalent character of the metal-boron cage bonds. Specifically, the shape of the frontier occupied MOs indicates that most of the MOs correspond to metal-ligand σ-bonding, primarily attributed to interactions of 5f orbitals of the actinides and 2p orbitals of the boron atoms. On the contrary, the MOs almost delocalized on the boron cages are found to be very low in energy, and the lowest unoccupied molecular orbitals LUMO and LUMO+1 represent metal-ligand σ-antibonding. For C_{2h} U@B_{36}, the two SOMOs, SOMO(a_u) and SOMO-1(b_u), correspond to U-B σ-bonding, mainly originating from the U 5f, 7p and B 2p orbitals. The two σ-bonds comprise 27 and 76% U 5f, and only 1 and 3% U 7p orbital character, respectively. The MOs ranging from HOMO(b_u) up to HOMO-4(a_u) are also metal-ligand σ-bonding. The MOs immediately below, i.e. HOMO-5(a_g), are essentially due to interactions of B 2p orbitals with slight contributions of U 6d orbitals. LUMO(b_g) and LUMO+1(b_g) are U-B σ-antibonding with 2% and 9% U 6d orbital contributions, respectively. The MOs of C_{2h} Th@B_{38} show similar character to those of C_{2h} U@B_{36} though the MO energies of Th@B_{38} are deeper than those of U@B_{36}, except for SOMO(b_u) and SOMO-1(a_g).

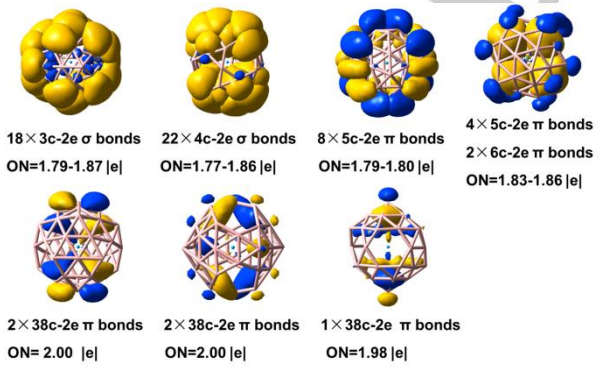

Figure 4. Bonding pattern of the global minimum C_{2h} Th@B_{38} from AdNDP analysis with the occupation numbers (ONs) indicated

Based on the calculated nucleus-independent chemical shifts (NICS)[20], C_{2h} Th@B_{38} possesses three-dimensional (3D) aromaticity with an NICS value of -274 ppm at the center of the B_{38} cage, while U@B_{36} seems to be antiaromatic (NICS: 5404 ppm). The aromaticity of C_{2h} Th@B_{38} can be further demonstrated from the chemical bonding analysis by the adaptive natural density partitioning (AdNDP). AdNDP, developed from natural bond orbital (NBO)[21-24] analysis, characterizes the *n*-center two-electron (*n*c-2e) bonding of a molecule with the range of *n* from one up to the total number of atoms in the molecule. Thus, the AdNDP analysis reveals the conventional Lewis bonds (lone pairs and 2c-2e bonds), as well as the nonclassical delocalized bonding (*n*c-2e).

As depicted in Figure 4, for the 59 pairs of valence electrons in Th@B_{38}, there are 40 delocalized σ bonds: 18 3c–2e σ bonds on the 18 B_3 triangles and 14 4c–2e σ bonds on the 14 B_3 triangles along with the central Th atom, and 8 on the quasi-planar jam-packed B_4 quadrangles on the B_{38} cage surface. Given that the 4c-2e σ bonds have considerable contributions from the B_3 triangles, the 40 σ frameworks can be considered as 40 3c-2e σ bonds. Thus, each B_3 triangle on the B_{38} cage surface possesses one 3c-2e σ bond. The remaining 38 valence electrons construct the π framework, involving four 5c–2e and two 6c–2e π bonds at the top and bottom of the cage, and eight 5c–2e π bonds around the waist, as well as five 38c–2e π bonds completely delocalized over the entire B_{38} cage surface. Consequently, all 118 valence electrons in Th@B_{38} take part in either delocalized σ or π covalent bonds, conforming to the general bonding pattern of σ + π double delocalization of the borospherene family. Apart from partial 4c–2e σ bonds with small participation of the central Th atom, the five 38c–2e π bonds also have minor involvement of Th. This bonding picture contrasts to the alkali-metal-doped borospherenes, such as Ca@B_{40}[8] and Ca@B_{38}[3], in which the Ca atoms are not involved in the σ + π double delocalization bonding, based on AdNDP analysis.

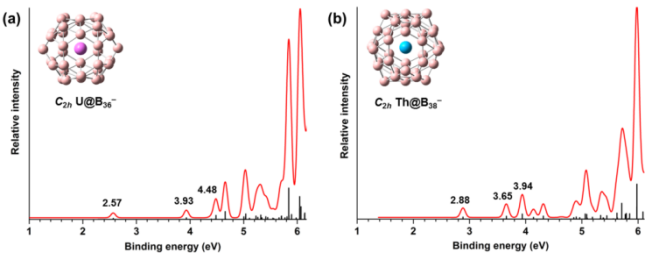

Figure 5. Simulated photoelectron spectrum of (a) C_{2h} U@B_{36}^- and (b) C_{2h} Th@B_{38}^- at the PBE0/RECP/6-311+G* level of theory

To aid future experimental characterization of the C_{2h} U@B_{36} and C_{2h} Th@B_{38} endohedral borospherenes, the photoelectron spectroscopy (PES) spectra of the monoanions C_{2h} U@B_{36}^- and Th@B_{38}^- were simulated using time-dependent DFT (TD-DFT). As displayed in Figure 5, the predicted first vertical detachment energies (VDE) and adiabatic detachment energies (ADE) are respectively 2.57 and 2.15 eV for U@B_{36}^-, and 2.88 and 2.49 eV for Th@B_{38}^-, which are weak predicted PES bands that arise

from the detachment of the electron from the SOMOs. There are relatively sizable energy gaps of 1.64 and 0.77 eV between the first and the second bands for $U@B_{36}^-$ and $Th@B_{38}^-$, respectively, reflecting the high electronic stabilities of the neutral species. The predicted vertical ionization potentials of $U@B_{36}$ and $Th@B_{38}$ are relatively high (6.10 and 6.11 eV), which are comparable to that of C_s $Ca@B_{38}$ (7.35 eV)[3] and further indicate high thermodynamic stability of these actinide borospherenes. The C_{2h} $U@B_{36}^{2-}$ and $Th@B_{38}^{2-}$ dianions seem to be less thermodynamically stable compared to $U@B_{36}^-$ and $Th@B_{38}^-$, with calculated ADEs for both of ~–0.8 eV at the PBE0 level (Figures S10 and S11). The main infrared (IR) absorption spectra features of the C_{2h} B_{36} and D_{2h} B_{38} cages in C_{2h} $U@B_{36}$ and C_{2h} $Th@B_{38}$ (Figure S12) could also promote and assist future experimental explorations of actinide endohedral borospherenes.

In summary, our calculations validated the viability of actinide borospherenes. The actinide size (atomic radii) appears to be crucial in forming stable actinide endohedral borospherenes. The B_{40} borospherenes can be stabilized by larger actinide metal atoms, such as Ac (atomic radii: 1.88 Å). The reported $U@B_{40}$ seems to fulfill the stable 32-electron configuration.[13] In contrast to alkaline earth metalloborosphenes, for example, covalent character bonding between actinides and the boron cages is an essential factor for the stability of actinoborspherenes. The current results demonstrate the possibility of chemical modification and functionalization of the boron fullerenes by doping with actinide metal atoms, thereby enhancing their stabilities and modifying surface reactivity. In view of the diversity of the borospherenes, we will further investigate stabilization of various borospherenes by doping with Th, U and other actinides.

Acknowledgements

This work was supported by the National Natural Science Foundation of China (Grant No. 11575212), the Major Research Plan “Breeding and Transmutation of Nuclear Fuel in Advanced Nuclear Fission Energy System” of Natural Science Foundation of China (Grant Nos. 91426302, 91326202), and the Science Challenge Project (JCKY2016212A504). J.K.G. was supported by the U.S. Department of Energy, Office of Basic Energy Sciences, Heavy Element Chemistry at LBNL under Contract No. DE-AC02-05CH11231. The results described in this work were obtained on the ScGrid of Supercomputing Center, Computer Network Information Center of Chinese Academy of Sciences.

Keywords: actinides • aromaticity • borospherenes • Density functional calculations • metalloborospherenes

[1] H. J. Zhai, Y. F. Zhao, W. L. Li, Q. Chen, H. Bai, H. S. Hu, Z. A. Piazza, W. J. Tian, H. G. Lu, Y. B. Wu, Y. W. Mu, G. F. Wei, Z. P. Liu, J. Li, S. D. Li, L. S. Wang, *Nat. Chem.* **2014**, *6*, 727-731.

[2] Q. Chen, W. L. Li, Y. F. Zhao, S. Y. Zhang, H. S. Hu, H. Bai, H. R. Li, W. J. Tian, H. G. Lu, H. J. Zhai, S. D. Li, J. Li, L. S. Wang, *ACS Nano* **2015**, *9*, 754-760.

[3] Q. Chen, H. R. Li, C. Q. Miao, Y. J. Wang, H. G. Lu, Y. W. Mu, G. M. Ren, H. J. Zhai, S. D. Li, *Phys. Chem. Chem. Phys.* **2016**, *18*, 11610-11615.

[4] W. J. Tian, Q. Chen, H. R. Li, M. Yan, Y. W. Mu, H. G. Lu, H. J. Zhai, S. D. Li, *Phys. Chem. Chem. Phys.* **2016**, *18*, 9922-9926.

[5] Q. Chen, S. Y. Zhang, H. Bai, W. J. Tian, T. Gao, H. R. Li, C. Q. Miao, Y. W. Mu, H. G. Lu, H. J. Zhai, S. D. Li, *Angew Chem Int Edit* **2015**, *54*, 8160-8164.

[6] J. Lv, Y. C. Wang, L. Zhu, Y. M. Ma, *Nanoscale* **2014**, *6*, 11692-11696.

[7] J. R. Heath, S. C. Obrien, Q. Zhang, Y. Liu, R. F. Curl, H. W. Kroto, F. K. Tittel, R. E. Smalley, *J. Am. Chem. Soc.* **1985**, *107*, 7779-7780.

[8] H. Bai, Q. Chen, H. J. Zhai, S. D. Li, *Angew Chem Int Edit* **2015**, *54*, 941-945.

[9] Q. Chen, T. Gao, W. J. Tian, H. Bai, S. Y. Zhang, H. R. Li, C. Q. Miao, Y. W. Mu, H. G. Lu, H. J. Zhai, S. D. Li, *Phys. Chem. Chem. Phys.* **2015**, *17*, 19690-19694.

[10] P. Jin, Q. H. Hou, C. C. Tang, Z. F. Chen, *Theor. Chem. Acc.* **2015**, *134*.

[11] Q. L. Lu, Q. Q. Luo, Y. D. Li, S. G. Huang, *Phys. Chem. Chem. Phys.* **2015**, *17*, 20897-20902.

[12] J. Lv, Y. C. Wang, L. J. Zhang, H. Q. Lin, J. J. Zhao, Y. M. Ma, *Nanoscale* **2015**, *7*, 10482-10489.

[13] T. Yu, Y. Gao, D. Xu, Z. Wang, *Nano Res.* **2017**, DOI 10.1007/s12274-12017-11637-12279.

[14] J. G. Speight, *Lange's handbook of chemistry*, 16th ed., McGraw-Hill, New York, **2005**.

[15] P. Pyykkö, M. Atsumi, *Chem. Eur. J.* **2009**, *15*, 12770-12779.

[16] C. F. Guerra, J. W. Handgraaf, E. J. Baerends, F. M. Bickelhaupt, *J. Comput. Chem.* **2004**, *25*, 189-210.

[17] F. L. Hirshfeld, *Theor. Chim. Acta* **1977**, *44*, 129-138.

[18] G. J. Cao, W. H. E. Schwarz, J. Li, *Inorg. Chem.* **2015**, *54*, 3695-3701.

[19] J. P. Dognon, C. Clavaguera, P. Pyykkö, *J. Am. Chem. Soc.* **2009**, *131*, 238-243.

[20] P. V. Schleyer, C. Maerker, A. Dransfeld, H. J. Jiao, N. J. R. V. Hommes, *J. Am. Chem. Soc.* **1996**, *118*, 6317-6318.

[21] J. E. Carpenter, F. Weinhold, *J. Mol. Struct. (THEOCHEM)* **1988**, *169*, 41-62.

[22] J. P. Foster, F. J. Weinhold, *J. Am. Chem. Soc.* **1980**, *102*, 7211-7218.

[23] A. E. Reed, R. B. Weinstock, F. Weinhold, *J. Chem. Phys.* **1985**, *83*, 735-746.

[24] A. E. Reed, L. A. Curtiss, F. Weinhold, *Chem. Rev.* **1986**, *6*, 899-926.

Entry for the Table of Contents (Please choose one layout)

Layout 1:

COMMUNICATION

Text for Table of Contents

Extensive first-principles theory calculations on AnB_n (An= U, Th; n=36, 38, 40) reveal the feasibility of actinide-doped borospherenes. Ultrastable $U@B_{36}$ (C_{2h}, ^3A_g) and $Th@B_{38}$ (C_{2h}, ^3B_u) exhibit almost perfect endohedral configurations with some covalency of the An-B bonds. $Th@B_{38}$ possesses 3D aromaticity involving a non-negligible contribution of the actinide metal center.

*Cong-Zhi Wang, Tao Bo, Jian-Hui Lan, Qun-Yan Wu, Zhi-Fang Chai, John K. Gibson, and Wei-Qun Shi**

Page No. – Page No.

Ultrastable Actinide Endohedral Borospherenes: $U@B_{36}$ and $Th@B_{38}$